PROCEEDINGS, 23rd Annual PNOC-EDC Geothermal Conference
Hotel Inter-Continental,Makati City, Philippines, March 13-14,2002

SILICA DEPOSITION ALONG KIRIOHINEKAI STREAM, WAIRAKEI, NEW ZEALAND

Ana C. Ragragio-Panopio

PNOC Energy Development Corporation, Merritt Road, Fort Bonifacio, Metro Manila 1201, Philippines

ABSTRACT

This study was undertaken to determine the rate and mechanisms of silica deposition along a 3 km segment of the Kiriohinekai Stream located within Wairakei Geothermal Field. Water samples from six sampling sites were collected for silica (total and monomeric) and colloid particle analysis. Representative silica deposits from the corresponding sampling site were also collected for XRD and XRF analysis.

The pH of the brine remained almost constant, which is about 8.6 while the temperature decreased from 77 to 32 "C along the stream. On the other hand, monomeric silica decreased significantly from 553 ppm to 205 ppm while total silica concentration declined slightly from 565 ppm to 493 ppm. The highest drop in total Si02 was between sampling sites US and TC in the upstream area with a deposition rate of 8.4 g/km-s. Particle size determination showed that the colloidal particle grew from 14 nm to 23 nm. The mineralogy of the deposits as given by XRD and XRF analysis are mainly amorphous silica with composition of between 88-97% SiO2, respectively.

The mechanism responsible for silica deposition in Kiriohinekai Stream apparently involves a condensation reaction (polymerization) catalyzed by hydroxyl ions. Formation of colloidal particles involves decrease in the monomeric silica concentration as a function of temperaturn and degree of supersaturation. The decrease in monomeric silica downstream corresponds to the amount of colloidal silica formed, which is capable of depositing on the streambed. The negligible silica deposition at distal downstream sites is related to particle size. Particles with diameter <20 nm deposit more quickly at temperatures ranging from 77 to 55 "C. Decline in monomeric silica due to polymerization is associated with changes in the morphology of the silica deposits.

1.0 INTRODUCTION

The aim of this project is to determine the rate and mechanism of silica deposition along the Kiriohinekai Stream, located within the Wairakei Geothermal Field. It is about 3 km long and about 1 to 5 m width. The stream was once naturally flowing and predominantly geothetmal fed by the outlet of the thermal features of Alum Lake and the Waiora Valley. Some time before the 1950's, the natural flow of this stream was diverted to a set of pools known as the Honeymoon Pools and then returned to the streambed approximately 200 meters downstream.

Originally, these thermal features discharged chloride waters from the Waiora Valley to the Kiriohinekai Stream. These no longer flow, and in order to replicate the original stream water volume and chemistry, Contact Energy transmits some of the separated bore water into the stream. Some of the geothermal brine from the Wairakei drain flows to the Kiriohinekai Stream where it travels much of its length. Before reaching the Waikato River, the flow is diverted to the Wairakei Stream via an existing artificial channel.

With the flow of geothetmal brine, silica deposits in the streambed at variable rate along the channel. Contact Energy promotes deposition of silica sinter and sinter terraces, which can be used as a tourist attraction. The processes described herein relate to understanding the mechanisms of silica deposition occurring in Kiriohinekai Stream. This may assist estimates of the rate of silica deposition in the stream.

Figure 1 shows the site location and the sampling sites. The discharge area is the main source of water. The oufflow drains to the east to Wairakei stream, which then flows to Waikato River.

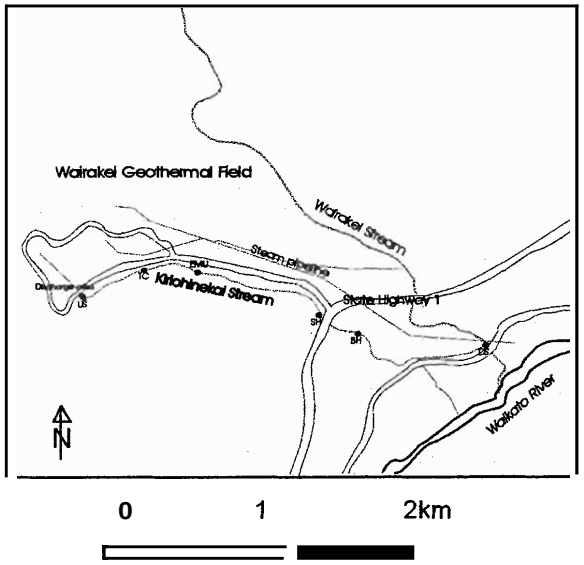

Figure 1. Sampling locations at Kiriohinekai Stream.

1.1 Silica Deposition

There are *two* mechanisms that lead to silica deposition (Henley, 1984):

Molecular deposition. Dissolved silica (H_4SiO_4, $H_3SiO_4^-$) bonds directly onto a growth surface. The rate of deposition is a function of temperature, supersaturation and the surface density of ionized silanol (-Si-OH) groups that, by itself, is a function of salinity and pH. Fluid flow rates may contribute to the deposition rate through the rate of supply of supersaturated solution to the growth site both through the bulk flow of fluid and the hydrodynamic control on the boundary layer thickness in the flow regime under consideration.

Homogeneous nucleation. Dissolved silica proceeds through a series of condensation reactions to form high molecular weight polymers, which then flocculate to form a low-density silica scale. Polymerization of silica involves condensation reactions of silanol groups:

$$-Si-Si-OH + HO-Si- \Leftrightarrow -SiOSi- + H_2O \quad (1)$$

The variables that control this process are supersaturation, temperature, and the surface tension of the silica-water interface.

Silica can be deposited molecularly from supersaturated aqueous solution. Supersaturation can be brought about by one of the following processes (Iler, 1979):

a. Concentrating an undersaturated solution by evaporating water.
b. Cooling a hot saturated solution in water.
c. Lowering the pH of an aqueous solution of a sotuble silicate below 10.7.
d. Generating $Si(OH)_4$ in water by hydrolyzing a monomeric silica compound.

Usually colloidal silica deposits are dense, vitreous, hard and often dark colored compared to low density silica 'floc' which accumulates in weirboxes and drains. When the solution cools, the colloidal particles deposit on solid surfaces while at the same time the solution becomes supersaturated with silica, which then deposits on the layer of deposited colloidal particles, cementing them together.

1.2 Particle Size Determination

The deposition rate of amorphous silica is related to the size of the particles suspended in the brine. This study used a MICROTAC Ultrafine Particle Size Analyzer that is based on the following theory of operation. The method of particle size analysis is based on the principle of Doppler effect and Brownian motion. The velocity distribution is a known function of particle size where the mean velocity of the particles in a sample is inversely proportional to the particle size. Light incident on a particle scatters in all directions. Moving particles suspended in the fluid are subject to random collisions. The moving particle shifts the frequency of scattered light by an amount proportional to the particle velocity. The Doppler frequency shift is detected and the output is digitized and mathematically analyzed to compute the frequency spectrum. Frequency shift is directly proportional to particle velocity distribution, which is a function of the particle size distribution.

1.3 X-ray Diffraction

X-ray diffraction (XRD) is a reliable and rapid technique for the precise determination of crystal structures. Powder diffractometers usually use samples mounted in flat-plate holders. The holder is rotated through the range of 2Φ values at a rate w, while the detector is rotated at the rate 2ω so that it is always in position to receive diffracted beams from planes at the proper angle

2ω. The signal from the detector is processed electronically and displayed as a pattern showing diffraction maxima as peaks, which is characteristic for the specimen (Griffen, 1992). This study used x-ray diffraction to determine the degree of crystallinity of the silica samples from the stream.

1.4 X-ray fluorimetry

X-ray fluorescence (XRF) is used mainly for bulk chemical analysis of rocks, soils, and sediments (Gardner, 1990). It is based on the irradiation of a sample by a primary X-ray beam. The individual atoms are excited emitting secondary X-rays that can be detected and recorded in a spectrum. The spectral lines or peaks of this spectrum are characteristic of the individual atoms i.e., of the respective elements present in the sample so that, by an appropriate interpretation of the spectrum, the sample can be analyzed (Klockenkamper, 1997). Different elements have different detection limits however, it is possible to detect concentrations as small as 1 ppm or less by XRF. On the other hand, XRF instrument requires at least 10'' g of material (Griffen, 1992). XRF analysis of the silica deposits was undertaken to determine the trace metals present in the samples.

2.0 EXPERIMENTAL METHODS

2.1 Sample Collection

Water samples were taken at five locations, namely: upstream (US), training center (TC), near EMU (EMU), near the road (SH1), behind the hctel (BH) and downstream (DS), of the Kiriohinekai Stream. Two samples were collected at each location. One sample was acidified with 1N HCl and the other was filtered using 0.45 µm Millipore filter paper after adding 10 drops of 50% HNO_3. The water samples were transferred into 100 ml sampling bottle. The pH and temperature at each sampling site were measured.

Silica deposits were collected from each sampling site for XRD and XRF analysis. Representative fist-sized samples were taken from the middle part of the stream.

2.2 Sample Analysis

Monomeric silica. The samples acidified with 1N HCI were used in the analysis for monomeric silica, determined by the UV-Vis spectrophotometric method. The method involves the reaction of molybdic acid with monomeric silica to give yellow silicomolybdic acid, which forms below about pH 2.5.

The following stock solutions were prepared for the analysis:
SiO_2 stock standard: 2140 ppm (1000 ppm Si); SiO_2 working standard: 214 ppm (100 ppm Si); Molybdate stock solution: 100 g/l ammonium heptamolybdate and 47 g/l concentrated ammonium hydroxide; Sulfuric acid solution: 1.5 N.

Molybdic acid reagent was prepared by mixing 100 ml of molybdate stock solution, 500 ml distilled water and 200 ml of 1.5N sulfuric acid. The reagent was made fresh during the time of the analysis.

To 20 ml of this reagent, 2, 4 and 6 ml of SiO_2 working standard solution was added and diluted with distilled water to 25 ml to prepare 214, 428 and 642 ppm solution, respectively. Two ml of sample was'also added with molybdic acid reagent. A reagent blank was included with the batch of samples. The absorbance was measured after 10 minutes at a wavelength of 410 nm. A calibration curve was produced to calculate the monomeric silica concentration of the samples.

Total Silica. The filtered, acidified samples were analyzed for total silica using atomic absorption spectrophotometric method.

The instrument settings are the following:
Lamp current: 12 mA; Wavelength: 251.6 nm; Slit width: 0.2 nm; Flame: N_2O / C_2H_2; Oxidant Flow: 3.75; Fuel Flow 5.0 - 5.5.

The following solutions were prepared for the analysis:

Si02 stock standard: 2140 ppm (1000 ppm Si); SiO_2 working standard: 214, 642 and 1070 ppm (100, 300, and 500 ppm Si); Matrix stock solution: 127.106 g AR NaCl and 17.161 g AR KCI in 1L (50,000 ppm Na / 9,000 ppm K); NaOH/EDTA solution: 0.125 N NaOH and 1250 ppm EDTA.

Site	pH (field)	Temp °C	Length m	$tSiO_2$ ppm	$mSiO_2$ ppm	C_{eguil} ppm	SSI	Mono Total
US	8.58	77	0	565 ± 2	553 ± 5	270	2.0	0.98
TC	8.64	63	345	530 ± 6	372 ± 1	221	1.7	0.70
EMU	8.62	55	615	532 ± 2	305 ± 2	196	1.6	0.57
SH	8.63	46	1148	537 ± 5	272 ± 2	169	1.6	0.51
BH	8.60	43	1793	53525	249 ± 1	160	1.6	0.47
DS	8.58	32	3000	4932 1	205 ± 1	134	1.5	0.42

The 214, 642, and 1070-ppm working standards were prepared by diluting the 100, 300 and 500 ml stock solution, respectively, to 1 liter. 20 ml of matrix stock solution was added to the working standards to give 1000-ppm Na/180 ppm K in final solution.

To 40 ml NaOH/EDTA solution, 10 ml of sample/standard solution was added. Control water was also treated the same way as the sample/standard solution. The alkaline solution stabilizes silica in the form of $H_3SiO_4^-$ while the EDTA complex calcium, which can interfere with the analysis.

The Varian Spectra AA-20 was optimized at 251.6 ηm wavelength and made sure that the more intense first line of the doublet was used. Calibration curve was produced to calculate the total silica concentration of the samples.

Particle Size. About 3 – 4 ml sample was transferred to the sample cell/compartment using a dropper. Each run takes 3 minutes to complete. The operation is computer controlled and the results can be stored and retrieved for printout of particle size distribution in tabulated form or histogram plot.

X-ray *Diffraction.* A portion of the silica samples was oven dried at 30°C before crushing with a mortar and pestle until the particles are fine. The particles are further powdered using a grinder prior XRD analysis. The finely ground powder was packed into an aluminum holder with an aperture of 10 x 20 x 1 mm and scanned from 10 – 40° 2θ at a scanning speed of 0.6°/minute and a slit width of 0.01° using CuKa radiation. The diffraction patterns were smoothed using the smooth function at 11 points using the Traces V6 software.

X-ray *Fluorimetry.* The samples were dried at 40°C to remove adsorbed water before weighing. About 20 g of sample was fragmented using a mortar and pestle. Then the particles are further ground to a fine powder using a mill with a tungsten carbide ring for about 10 minutes. Approximately 10 g of powdered sample were mixed about one ml of 2% polyvinylalcohol solution with a mortar and pestle. The sample mixture was poured into a stainless steel mold and pressed into a disc at a pressure of –500 psi. The sample disc was immediately placed in a drying oven at 50°C to allow the X-ray transparent polyvinyl cement to harden. Spectro Plus Software using semi-quantitative calibration standards was used for the analysis. The output spectrum was interpreted by identifying the individual peaks produced.

2.0 RESULTS AND DISCUSSION

2.1 Total and Monomeric Silica Composition

The results of total and monomeric silica analyses were listed in Table 1. All values for silica concentrations were average of two values. The pH of the water remained almost constant throughout the stream, which is about 8.6. However, the temperature of the brine decreased from 77°C to 32°C as it flows downstream. The monomeric silica of this brine decreased significantly from an upstream value of 553 ppm SiO_2 to a downstream value of 205 ppm SiO_2. The decrease in total silica from sample site US to sample site TC is 34 ppm. This corresponds to the concentration of silica that deposited. However, the slight variability in the total silica content of the brine from sample site TC to sample site BH corresponds to the uncertainty of analytical method, which is ± 2%. The result of the total silica at the sample site

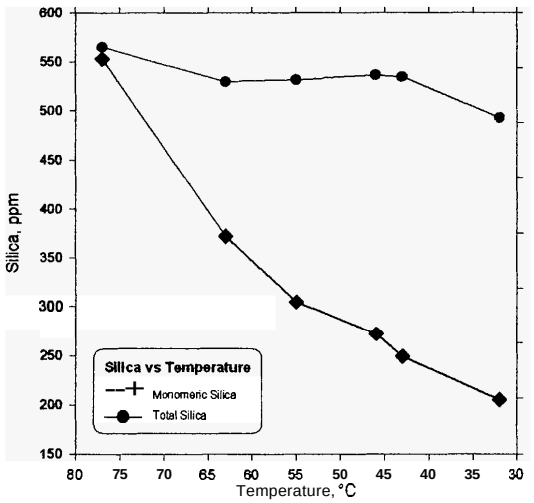

Figure 2. Monomeric/total silica along the Kiriohinekai Stream.

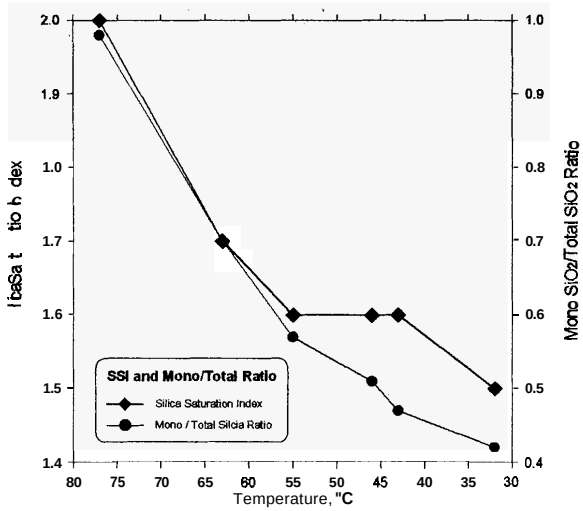

Figure 3. SSI along the Kiciohinekai Stream.

DS is ambiguous because it is expected that its total silica concentration will not vary compared to the previous sampling site (BH) because of negligible deposition in sample site DS. The cause of this instance is probably due to analytical error. Figure 2 shows the total and monomeric silica in relation to the temperature and distance from the discharge area. The decline in monomeric silica is due to formation of colloidal silica as a result of the fast cooling of the hot saturated geothermal brine as it flows to the stream. When the solution cools, the colloidal particles are deposited on solid surfaces at the same time the cooled solution becomes supersaturated with silica, which is then deposited on the layer of deposited colloidal particles, cementing them together (Iler, 1979). But in this case, the deposition significantly decreased as the solution cooled. This could be attributed to the decrease in silica saturation index (monomeric silica concentration divided by equilibrium amorphous silica solubility). Table 1 also shows the rate of disappearance of monomer as seen on the decline of the monomeric silica to total silica concentration ratio. This gives us the idea of the rate of formation of colloidal particles. It suggests that the monomeric silica polymerizes and decreases in concentration very rapidly as the brine flows downstream and cools. Colloidal growth is directly correlated to the decreasing concentration of monomeric silica, which results to silica deposition upstream. In Figure 3, the amount of monomer in solution is drawn as a function of temperature. The figure shows the decline in the amount of unreacted monomer as the temperature decreased due to the drop in activation energy of polymerization. Although the effect of decreasing temperature on the polymerization rate is difficult to determine because changing the temperature also changes the degree of supersaturation, the data suggest that there is a decrease in polymerization rate with a decrease in temperature. This is expected based on principles of chemical reactions.

2.2 Particle Size

Water samples from upstream (US), near the EMU (EMU), and downstream (DS) were measured for colloid partide size using the Microtac Ultrafine Particle Analyzer. The results of particle size distribution of silica in the water samples collected from the stream are listed in Table 2. It shows that the particle size grew from 14 nm to about 23 nm from upstream to downstream. Figure 4 shows the increase in average particle size of colloidal silica as the concentration of monomeric silica decreases. This trend is typical for silica polymerization where the particles increase in size at the same time decreases the concentration of monomer in equilibrium with these particles. The increase in

Location	Average Particle Size (nm)
US	14
EMU	**19**
DS	**23**

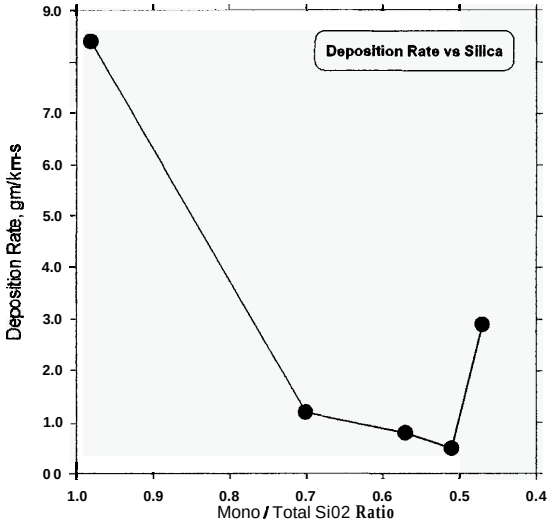

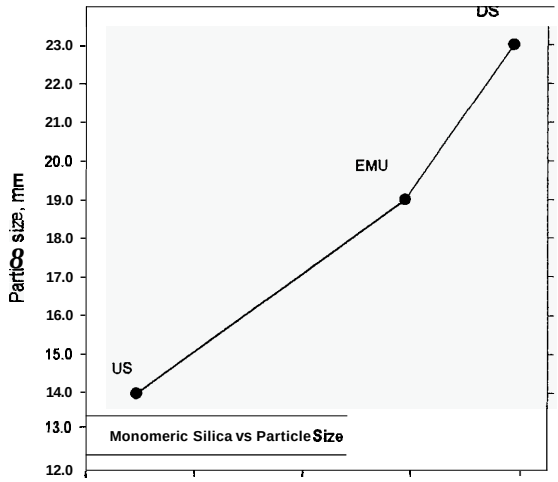

Figure 4. Deposition rate along Kiriohinekai Stream

average particle size continues until a critical size is reached. This is the size when the surface area is sufficiently large to prevent fusion of colloids and their subsequent deposition. Deposition is likely rapid when the colloidal particles are less than 5 nm in diameter and unlikely to occur if colloidal particles are larger than about 20 nm (Iler, 1979). Deposition of colloidal silica particles will be negligible with diameter of >20 ηm because small colloidal particles are much more likely to adhere to each other in suspension than to the surface. A study (Pott, et al, 1996) confirms this behavior where deposition rate is dependent of particle size, with small particles depositing more quickly; deposition rates rapidly decrease with distance from the discharge area. Thus, deposits are absent at the downstream sites of Kiriohinekai stream.

2.3 Deposition Rate

Since the fluid flow path is not uniform, silica deposition rate was difficult to determine. The average mass flow rate of the stream is about 300 tons/hr. The drop in total silica concentration of the water between two succeeding sampling points suggests the amount of silica deposited within in the area. The formula below was used was used to estimate the rate of deposition:

$$R = \frac{\Delta tSiO_2 \times M}{D} \qquad (2)$$

where:

R = deposition rate (g/km-s)
$\Delta tSiO_2$ = difference in $tSiO_2$ between sampling point
M = mass flow rate = 300 t/hr = 83.3 kg/s
D = distance between sampling points (km)

Table 3 shows the calculated drop in total silica concentration of the water and deposition rate between two succeeding sampling points. The difference in total silica between US and TC is 35 ppm which is equivalent to deposition rate of about 8.4 g/km-s. However, the difference in total silica at sample sites TC, EMU, SH and BH is insignificant compared to the uncertainty of the analytical method. This limits accurate quantification of the rate of silica deposition.

Table 3 Deposition Rates alona the stream.

Site	$\Delta tSiO_2$ ppm	Deposition Rate (g/s)	Deposition Rate (g/km-s)
US – TC	35.5 ± 5	2.92 ± 0.42	8.4 ± 1.2
TC – EMU	4 ± 2	0.33 ± 0.16	1.2 ± 0.6
EMU – SH	5 ± 4	0.42 ± 0.33	0.8 ± 0.6
SH – BH	4 f 3	0.33 ± 0.25	0.5 ± 0.4
BH – DS	42 ± 5	3.49 ± 0.42	2.9 ± 0.3

The data in Table 3 has been drawn in Figure 5. Except for the last data, the figure shows that deposition rate decreases as the ratio of monomeric silica to total silica decreases. This trend is reasonably consistent with the fact that the deposition rate is a function of the amount of

monomeric silica in the solution, which is a function of temperature. Colloidal silica deposited from supersaturated solution onto the streambed at a rate that decreases with decreasing degree of supersaturation with respect to amorphous silica at the temperature measured.

2.4 Morphology and Mineralogy of the Silica Deposits

Morphology. Moving downstream from the discharge area, the deposit morphology changed successively from very hard, dense and granular → compact with overlapping layers producing ripple texture, which relates to the direction of water flow at the time of deposition → massive, sponge-like, porous mass with layering of various shades of chalky white, light brown and light green silica → very soft porous dark brown → very soft sparse coating. There was negligibte sitica deposit at sample site DS. The deposits are very hard at sample site **US** due to cementation of colloidal aggregates. Alternating laminae of silica deposits with varying color may mark changes in the fluid flow rates. The change in color of the deposits from brown **(US)** to white (EMU) is most likely to be associated to the decreasing amount of dissolved H_2S in the brine which is incorporated with the silica upon deposition (Mroczek and Reeves, 1994). The change in morphology of the silica deposits seems to be related to the particle size, which is a function of the amount of monomeric silica in the water.

Mineralogy of silica deposits. The deposits are amorphous based on X-ray diffraction and were mainly Opal A, with some detritus minerals like quartz, cristobalite, and plagioclase (Table 4). There are unidentified peaks that may relate to other trace amounts of detritus minerals.

Table 4. Mineralogy of silica deposits from Kiriohinekai Stream.

Site	Opal A	Quartz	Cristobalite	Plagioclase
US	√		√	√
TC	√			√
EMU	√		√	√
SH	√	√	√	√
BH	√	√	√	

Note: √ - present

Degree of crystallinity of silica deposits. The position of maximum intensity was determined for each trace and the width of the peak at half-maximum intensity was calculated. The measured and calculated data for the samples are presented in Table 5. The width of the peak at half of the maximum intensity is a function of the degree of crystallinity of the silica deposits. For the samples collected in Kiriohinekai Stream, it suggests that the silica deposits are decreasing in degree of crystallinity downstream from the discharge area. This is in effect of decreasing temperature.

Site	Max intensity counts	Max intensity position	Width @ ½ max. intensity
US	124	3.95	7.25
TC	130	4.00	7.25
EMU	126	3.95	7.50
SH	114	3.98	8.75
BH	128	3.99	8.12

Composition of silica deposits. The results of XRF analysis are given in Table 6. Silica (SiO_2) content of the sample collected from the stream ranges between 88 to 97 % with the highest SiO_2 content from sample site **EMU** where the flow is less turbulent and minimal presence of transported materials. The remainder consists of Al_2O_3, Na_2O, Fe_2O_3, K_2O, CaO, and Cl in concentration range between 0.14 – 4.91%. The levels of other compounds like TiO_2, MnO, MgO, SO_3, Cu, Ga, Rb, Sb, Sr, Zn and Zr are very low (<0.17%). Br and Y are below the detection limit of 0.001% as is Ba, P_2O_5, and As for a detection limit of 0.01%, 0.0089% and 0.0068%, respectively. The presence of Al^{3+} and Fe^{3+} could be attributed to the substitution of alumino-silicates for Si^{4+} of the silica deposits. On the other hand, presence of Na_2O, K_2O, and CaO are associated with plagioclase feldspars derived from detritus minerals or from cations present in geothermal fluids.

Overall, the silica deposits in Kiriohinekai Stream are generally homogeneous entity with little variation in its mineralogy.

3.0 SUMMARY AND CONCLUSIONS

The mechanisms of silica deposition along Kiriohinekai Stream apparently involves a condensation reaction (polymerization) catalyzed by hydroxyl ions because the brine is above pH 8, which allows rapid formation of colloidat particles. Formation of colloidal

'able 6. Compo: ion of silica deposits from Kiriohinekai Stream

Compound	US (%)	TC	EMU	SH	BH
SiO_2	96.63	96.89	97.18	88.44	93.95
TiO_2	0.03	0.01	0.02	0.14	0.07
Al_2O_3	1.34	0.62	0.66	4.91	1.88
Fe_2O_3	0.28	0.25	0.29	1.24	0.67
MnO	0.02	0.01	0.01	0.03	0.02
MgO	0.03	0.06	0.05	0.11	0.06
CaO	0.48	0.28	0.27	0.95	0.60
Na20	0.59	0.77	0.63	1.77	0.96
K_2O	0.41	0.26	0.27	1.30	0.64
P_2O_5	<0.0089	<0.0089	<0.0089	0.04	0.03
SO_3	0.03	0.05	0.05	0.17	0.17
Ba	<0.010	<0.010	<0.010	0.03	0.01
Cl	0.14	0.80	0.56	0.84	0.91
As	<0.0068	<0.0068	<0.0068	<0.0068	<0.0068
Br	<0.001	0.0016	0.0010	0.0017	0.0030
c u	0.0063	0.0036	0.0032	0.0032	0.0036
Ga	0.0035	<0.0012	<0.0012	<0.0012	<0.0012
Rb	0.0044	0.0033	0.0031	0.0077	0.0057
Sb	0.0110	0.0061	<0.0061	<0.0061	<0.0061
Sr	0.0024	0.0010	0.0014	0.0079	0.0039
Y	<0.001	<0.001	<0.001	0.0019	0.0013
Zn	0.0030	0.0019	0.0019	0.0063	0.0041
Zr	0.0025	0.0008	0.0019	0.0120	0.0052

particles involves decrease in monomeric silica concentration that is a function of temperature and degree of supersaturation. The decrease in monomeric silica downstream corresponds to the amount of colloidal silica formed that is capable of depositing on the surface of the bed of the channel. The varying depositibn rate along the stream with virtually negligible deposition downstream is related to particle size, with small particles depositing more quickly, and that deposition rate rapidly decrease with distance from' upstream.

Since the flow of the water is not uniform, deposition rate was calculated based on the amount of drop in total silica along the stream. The maximum deposition rate occurred upstream where the temperature and degree of supersaturation with respect to amorphous silica are highest.

The change in morphology of the deposits from very hard and compact to very soft and porous is a result of the changes in the mode or rate of deposition. Colloidal particle size that is a function of rate of deposition also affected the morphology of the deposits.

The deposits are mainly amorphous silica based on X-ray diffraction with some detritus minerals present during deposition. The composition of the deposits as given by X-ray fluorimetry is mostly of SiO_2 (88 – 97%) with minimal levels of Al_2O_3 and Fe_2O_3. Presence of Na_2O and K_2O in low levels is derived from detritus plagioclase feldspars and cations present in the geothermal fluid.